

268, 700 (1995).

8. R. J. Tonucci *et al.*, *ibid.* **258**, 783 (1992).

9. D. Washington, V. Duchenois, R. Polaert, R. M. Beasley, *Acta Electron.* **14**, 201 (1971); J. L. Wisa, *Nucl. Instrum. Methods Phys. Res. Sect. A* **162**, 587 (1979).

10. We would like to acknowledge support from the

Office of Naval Research and the Advanced Research Projects Agency's Microelectronics Technology Office. D.H.P. would like to acknowledge support from the National Research Council's Research Associateship Programs.

16 May 1995; accepted 9 August 1995

## Emission Measurements of the Concorde Supersonic Aircraft in the Lower Stratosphere

D. W. Fahey, E. R. Keim, K. A. Boering, C. A. Brock, J. C. Wilson,\* H. H. Jonsson, S. Anthony, T. F. Hanisco, P. O. Wennberg, R. C. Miake-Lye, R. J. Salawitch, N. Louisnard, E. L. Woodbridge, R. S. Gao, S. G. Donnelly, R. C. Wamsley, L. A. Del Negro, S. Solomon, B. C. Daube, S. C. Wofsy, C. R. Webster, R. D. May, K. K. Kelly, M. Loewenstein, J. R. Podolske, K. R. Chan

Emission indices of reactive gases and particles were determined from measurements in the exhaust plume of a Concorde aircraft cruising at supersonic speeds in the stratosphere. Values for  $\text{NO}_x$  (sum of  $\text{NO}$  and  $\text{NO}_2$ ) agree well with ground-based estimates. Measurements of  $\text{NO}_x$  and  $\text{HO}_x$  indicate a limited role for nitric acid in the plume. The large number of submicrometer particles measured implies efficient conversion of fuel sulfur to sulfuric acid in the engine or at emission. A new fleet of supersonic aircraft with similar particle emissions would significantly increase stratospheric aerosol surface areas and may increase ozone loss above that expected for  $\text{NO}_x$  emissions alone.

Emissions from aircraft include many species that play a role in atmospheric chemical and radiative processes (1). Programs in the United States and other countries are under way to evaluate the effects of expanding the number of high-speed civil transport (HSCT) aircraft that operate in the stratosphere (2, 3). In addition to the severe

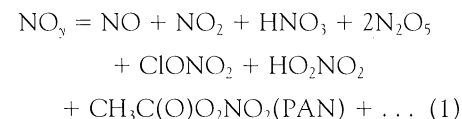
technical challenges that must be addressed, significant environmental issues related to the role of exhaust emissions in climate and global change must also be addressed before such a fleet can be considered viable (4). The emission requirements imposed on new engines will largely depend on the environmental consequences attributed to the emissions.

The HSCT aircraft will emit reactive nitrogen,  $\text{NO}_y$ , in the form of  $\text{NO}_x$  at altitudes in the lower stratosphere between 16 and 23 km while operating at speeds of Mach 1.6 to 3.2, respectively. The  $\text{NO}_x$  participates directly and indirectly in catalytic cycles that destroy  $\text{O}_3$  in the lower stratosphere (5). However, the sensitivity of  $\text{O}_3$  loss to  $\text{NO}_x$  emissions is reduced in atmospheric models when heterogeneous reactions on background sulfate aerosol particles are included (6–8), because the  $\text{NO}_x$  fraction of  $\text{NO}_y$  is reduced through more effective conversion to  $\text{HNO}_3$  (9). One current estimate is that the emission from a fleet of 500 HSCT aircraft operating in the year 2015 at Mach 2.4 (20 km) would change column  $\text{O}_3$  by less than 1% between 40° and 50°N if the emission index (EI) for  $\text{NO}_x$  is 15 g of  $\text{NO}_x$  per kilogram of fuel or less (7). Losses increase if either the EI for  $\text{NO}_x$  or the flight altitude are increased. However, these calculations currently do not include the effects of the

emission of sulfate particles.

To date, no direct EI measurements for reactive nitrogen species or particles have been reported for a supersonic aircraft operating in the stratosphere. Instead, EI values for  $\text{NO}_x$  are derived from ground-based engine measurements (10, 11). Particle emission parameters are not well characterized for supersonic aircraft operating in the stratosphere, because ground-based tests do not fully simulate the growth and coagulation processes in the plume that change particle number, size, and composition after the engine exhaust enters the surrounding atmosphere. We present here measurements made behind the Concorde aircraft and use them to address  $\text{NO}_x$  and particle emission rates, the formation of nitric and sulfuric acid in the exhaust plume, and the potential consequences of particle emission for  $\text{O}_3$  loss calculations.

The Concorde exhaust was sampled on 8 October 1994, off the coast of New Zealand (Fig. 1). A 320-km section of the flight path traversed by the Concorde in 10 min at Mach 2 was sampled by the NASA ER-2 aircraft in three 30-min segments, during which the ER-2 moved back and forth across the path at different altitudes. The plume was encountered at least 11 times during this period (Fig. 2). The gas and particle instruments on board the ER-2 are well suited to analyze aircraft exhaust: all have a sampling rate of 0.3 Hz or higher and have demonstrated precision and accuracy in measurements in the background atmosphere (12) (Table 1). A  $\text{CO}_2$  measurement in the plume provided the dilution factor because  $\text{CO}_2$  can be directly related to fuel use from the stoichiometry of combustion. This dilution factor allows measurements of other species to be expressed as EIs. The reactive nitrogen instrument provided separate measurements of  $\text{NO}$  (the primary nitrogen emission), the secondary product  $\text{NO}_2$ , and  $\text{NO}_y$ ;  $\text{NO}_y$  is the reservoir of reactive nitrogen species



(PAN, peroxyacetyl nitrate) measured through catalytic conversion to  $\text{NO}$  and detection of  $\text{NO}$  using chemiluminescence. With a measure of  $\text{NO}$  and  $\text{NO}_y$ , the conversion of  $\text{NO}$  to higher oxides can be monitored in the plume. Other gaseous combustion products include  $\text{H}_2\text{O}$ , also directly related to the quantity of fuel burned, and  $\text{CO}$ , which is related to the efficiency of combustion. We used  $\text{N}_2\text{O}$  as a reference to the background atmosphere because it is a long-lived species in the stratosphere and significant  $\text{N}_2\text{O}$  production is not expected in the engine (11, 13). Measurements of

D. W. Fahey, E. R. Keim, S. Solomon, K. K. Kelly, Aeronomy Laboratory, National Oceanic and Atmospheric Administration (NOAA), Boulder, CO 80303, USA.

K. A. Boering, B. C. Daube, S. C. Wofsy, Department of Earth and Planetary Sciences, Harvard University, Cambridge, MA 02138, USA.

C. A. Brock, J. C. Wilson, H. H. Jonsson, Department of Engineering, University of Denver, Denver, CO 80208, USA.

S. Anthony, Cooperative Institute for Research in Environmental Science (CIRES), University of Colorado, Boulder, CO 80309, USA.

T. F. Hanisco and P. O. Wennberg, Department of Chemistry, Harvard University, Cambridge, MA 02138, USA.

R. C. Miake-Lye, Aerodyne Research, Billerica, MA 01821, USA.

R. J. Salawitch, C. R. Webster, R. D. May, Jet Propulsion Laboratory, Pasadena, CA 91109, USA.

N. Louisnard, Office National d'Études et de Recherches Aérospatiales (ONERA), Paris, France.

E. L. Woodbridge, Scripps Institution of Oceanography, University of California at San Diego, La Jolla, CA 92093, USA.

R. S. Gao, S. G. Donnelly, R. C. Wamsley, L. A. Del Negro, NOAA Aeronomy Laboratory, Boulder, CO 80303, and CIRES, University of Colorado, Boulder, CO 80309, USA.

M. Loewenstein, J. R. Podolske, K. R. Chan, National Aeronautics and Space Administration (NASA) Ames Research Center, Moffett Field, CA 94035, USA.

\*To whom correspondence should be addressed.

OH and HO<sub>2</sub> constrain the oxidation rates of sulfur and nitrogen species in the plume and, thus, the partitioning within the associated reservoirs. The total (nonvolatile + volatile) mixing ratio of aerosol particles and the nonvolatile fraction in the plume were determined with a two-channel condensation nuclei (CN) counter in which the inlet to the nonvolatile channel was heated to 192°C.

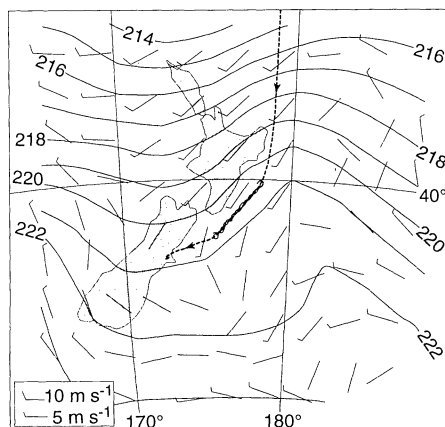


**Fig. 1.** Flight path (dashed line) of the Concorde from Fiji to Christchurch, New Zealand, on 8 October 1994. Temperature isolines and winds on the 100-mbar surface (altitude of 16.2 km) are from the NASA Goddard Space Flight Center assimilation model (33). The flight track of the ER-2 is superimposed on the Concorde track for the sampling segments. The Concorde produced no contrail visible from the ER-2 aircraft. Slack winds in the encounter region greatly simplified the sampling strategy because advection and shear effects were minimized. Operating conditions of the Concorde: Mach number, 1.97; computed air speed, 495 knots; fuel flow, 1.5 kg s<sup>-1</sup> engine<sup>-1</sup>; exhaust gas temperature, 680°C; engine rpm (N1-N4), 104%; ambient temperature, 222 K; and altitude, 16.1 km (100 mbar). Although afterburners are operated on all four engines during take-off and transonic acceleration, they are not used in supersonic cruise.

The principal encounter events are visible in the NO<sub>y</sub> data as short (<20 s) departures from a smooth, slowly varying background (Fig. 2). The events are also present in the CO<sub>2</sub> data, although the relative variability of the background is larger. The absence of N<sub>2</sub>O events is strong evidence that those in the NO<sub>y</sub> and CO<sub>2</sub> time series cannot be attributed to dynamical or chemical phenomena in the background atmosphere. In an expansion of the most intense encounter (event 3) (Fig. 3), the coincidence in time of the individual peaks further attests to the identity of the perturbation as aircraft exhaust. The age of the exhaust sampled in an event, as approximated from the location history of each aircraft, varies from 13 to 58 min. The dilution factor of the exhaust gas is about 3 × 10<sup>-5</sup> for 1 part per million by volume (ppmv) of CO<sub>2</sub> in the plume (11).

An accurate comparison of the abundances of emitted species requires that the event peaks are first integrated above background values. We calculated background

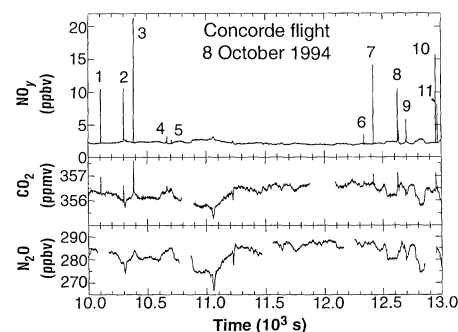


**Fig. 2.** Time series of measurements during the 1-hour interval that includes the 11 principal plume events shown as numbered peaks. Units are mixing ratio in parts per million by volume (ppmv) and parts per billion by volume (ppbv) for ambient conditions of 220 K and 100 mbar. The bottom axis indicates Universal Time on 8 October 1994.

CO<sub>2</sub> values during each event using the correlation of CO<sub>2</sub> with N<sub>2</sub>O observed on this flight and throughout the lower stratosphere (14). These estimated CO<sub>2</sub> values were then subtracted from measured values at each point before integration. Events 3, 7, and 8 (Table 2) were chosen for the EI calculations because they were least sensitive to the details of the integration step. Given the high accuracy and precision of individual CO<sub>2</sub> measurements (better than 0.1%), the overall accuracy of the CO<sub>2</sub> integration is estimated to be ±10% (1σ). The calculation of a species EI can be made once integrals for CO<sub>2</sub> and the species of

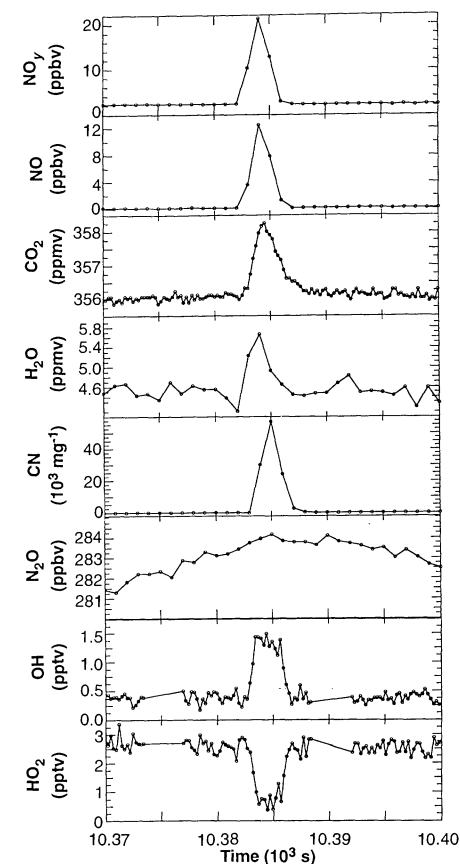


**Fig. 3.** Expanded time series of plume event 3, which has the largest peak values and integrals of all the events. Lines connect individual measurements (circles). The CN data are measured in thousands of nonvolatile particles per milligram of air that passed through the heated inlet. Ambient air density is 0.16 mg cm<sup>-3</sup>. The precise location of the peaks and the peak shapes for each species are not expected to be identical because each instrument monitors a species with a different combination of sample volume, sample residence time, signal integration period, and absolute time calibration. However, because each instrument is designed to provide a continuous measurement in a constant sample flow of ambient air, abundances can be compared as peak integrals (11). Although H<sub>2</sub>O values demonstrate the presence of the plume, they cannot be used quantitatively here because of wall adsorption (11). The bottom axis indicates Universal Time on 8 October 1994.

**Table 1.** Instrumentation on board the ER-2. Precision and accuracy are estimated. Pressure and temperature were sampled by aircraft probes each second with accuracies of ±0.3 mbar and ±0.3 K (34). UV, ultraviolet; IR, infrared.

Species	Technique	Sampling rate (Hz)	Residence time (s)	Precision (ppbv)	Accuracy (%)	Ref.
NO	NO/O <sub>3</sub> chemiluminescence	1	<1	±0.02	±15	(35)
NO <sub>2</sub>	UV photolysis and NO/O <sub>3</sub> chemiluminescence	1	1.5	±0.05	±15	(36)
NO <sub>y</sub>	NO/O <sub>3</sub> chemiluminescence	1	<1	±0.05	±20	(35)
CO <sub>2</sub>	IR absorption	4	1.5	±40	±0.1 ppmv	(14)
CO	Tunable diode-laser absorption	0.3	1.5	±1	±10	(37)
H <sub>2</sub> O	Lyman-α hygrometer	1	<1	±200	±10	(38)
CN	Growth chamber-light scattering	1	<1	±20*	±20	(39)
OH	Laser-induced fluorescence	8	<0.001	±0.00005	±30	(27)
HO <sub>2</sub>	Chemical conversion to OH	8	<0.001	±0.0002	±40	(27)
N <sub>2</sub> O	Tunable diode-laser absorption	1	2	±2.5%	±2.5	(40)
O <sub>3</sub>	UV absorption	1	1	±5%	—	(41)

\*Measured in particles per milligram of air.

interest are available and the carbon content of the fuel is known (15).

Using the  $\text{NO}_x\text{-N}_2\text{O}$  correlation (16) for background  $\text{NO}_y$  values in a manner similar to that used for  $\text{CO}_2$ , we obtained the  $\text{NO}_y$  integrals with an uncertainty of  $\pm 2\%$ . The EI values for the three selected events yielded an average of  $23.3 \text{ g NO}_x (\text{kg fuel})^{-1}$  with an uncertainty of  $\pm 20\%$  ( $1\sigma$ ) (Table 2). The accuracy of the  $\text{NO}_2$  integration was lower ( $\sim \pm 30\%$ ) because  $\text{NO}_2$  is measured as a difference signal within the  $\text{NO}_y$  detector system and no background estimation is available. The  $\text{NO}_x/\text{NO}_y$  ratios in the plumes were calculated in two ways (Table 2). In the first method, integrals of measured  $\text{NO}$ ,  $\text{NO}_2$ , and  $\text{NO}_y$  were used to form the  $\text{NO}_x/\text{NO}_y$  ratio directly. In the second method,  $\text{NO}_2$  was estimated from the photochemical steady-state relation involving the reaction of  $\text{NO}$  with  $\text{O}_3$  and photolysis of  $\text{NO}_2$  (17).

The EI for nonvolatile particles was calculated from a direct integral of CN event data, where the integral precision was better than 1%. The count rates for total particles were too large in the selected plume events to be recorded accurately because of counter saturation. As a result of the excellent signal/background ratio, weaker plume events that did not saturate either CN channel were observed. In these events, 70 to 90% of the particles were volatile at  $192^\circ\text{C}$ . Using this ratio as representative for the events in Table 2, we estimated the EI range for volatile particles to be  $(1.7 \text{ to } 6.5) \times 10^{17} (\text{kg fuel})^{-1}$ . In previous CN observations made in the stratosphere 18 hours after the passage of an SR-71 supersonic aircraft, the ratios of volatile to nonvolatile particles were similar to those reported here, and the EI for total CN was estimated to be  $(2 \text{ to } 9) \times 10^{16} (\text{kg fuel})^{-1}$  for particles larger than  $0.02 \mu\text{m}$  in diameter (18).

In theoretical and ground-based experimental studies of the Concorde Olympus 593 engine in the 1970s, the EI of  $\text{NO}_x$  received the most attention because of its recognized contribution to  $\text{O}_3$  loss rates (10, 19, 20). Experimental studies included emission tests in a pressure cell designed to simulate the temperature, pressure, and water vapor conditions of the stratosphere. The results of the present study agree well with previous test cell measurements (Table 2). The latter results are within the uncertainty bounds of  $\pm 20\%$  placed on the EI values determined here. Good agreement is also noted with semiempirical estimates of the  $\text{NO}_x$  EI, made from the functional dependence of  $\text{NO}_x$  production on compressor inlet temperature, pressure, and residence time and a single ground-based measurement for normalization (10). The overall agreement of the results from the Concorde plume with those of previous studies in-

**Table 2.** Concorde EI values. For comparison, previous experimental and theoretical results are also given.

Source	Plume age (min)	$\text{NO}_x/\text{NO}_y^*$	Emission indices (per kilogram of fuel)			
			$\text{NO}_y$ (g $\text{NO}_2$ )	$\text{CO}^\dagger$ (g CO)	Non-volatiles ( $10^{16}$ particles)	Volatiles ( $10^{17}$ particles)
Event 3	16	0.88 (1.06)	22.8	<3.5	4.3	—
Event 7	54	0.84 (1.08)	27.1	<3.5	8.7	—
Event 8	58	0.90 (1.11)	19.9	<3.5	8.5	—
Average	—	0.87 (1.08)	23.3‡	<3.5	7.2	1.7 to 6.5
CIAP (exp.) (42)	—	—	18.9–19.9	1.4–4.3	—	—
CIAP (theory) (42)	—	—	19.5–21.7	3.5	—	—
COVOS (exp.) (43)	—	—	23.2–26.5	2.4–4.6	—	—

\*Values in parentheses use steady-state  $\text{NO}_2$  calculated from Eq. 3. †No plume signal was evident in the time series of CO observations: If the signal-to-noise ratio in the CO data is used to limit the maximum allowable peak, the EI of CO must be less than ground-based measurements of  $3.5 \text{ g CO (kg fuel)}^{-1}$  (11, 19). The upper limit value is consistent with both previous studies and attests to the high efficiency of the Olympus 593 combustor. ‡The average  $\text{NO}_y$  EI had an uncertainty of  $\pm 20\%$ .

creases confidence that the emission of reactive nitrogen from a new supersonic HSCT engine operating in the stratosphere can be predicted adequately by ground-based techniques that could be used long before the first flight of the aircraft.

The direct  $\text{NO}_x/\text{NO}_y$  measurements yield an average of 0.9 (Table 2), confirming that the fraction of non- $\text{NO}_x$  species in the plume was small, as assumed in test cell and other ground-based measurements. In contrast,  $\text{NO}_x/\text{NO}_y$  values exceeded unity (Table 2) when the steady-state estimate of  $\text{NO}_2$  [Eq. 3 (17)] was used, because steady-state  $\text{NO}_2$  values in the plume were twice the measured values. Outside the plume, the difference was less than 10%. This discrepancy indicates that other reactions contribute to the steady-state balance inside the plume. The high  $\text{NO}_x/\text{NO}_y$  ratios indicate that  $\text{HNO}_3$ , a principal  $\text{NO}_y$  species and aerosol component in the stratosphere, was not abundant in the plume in the first minutes to hours.

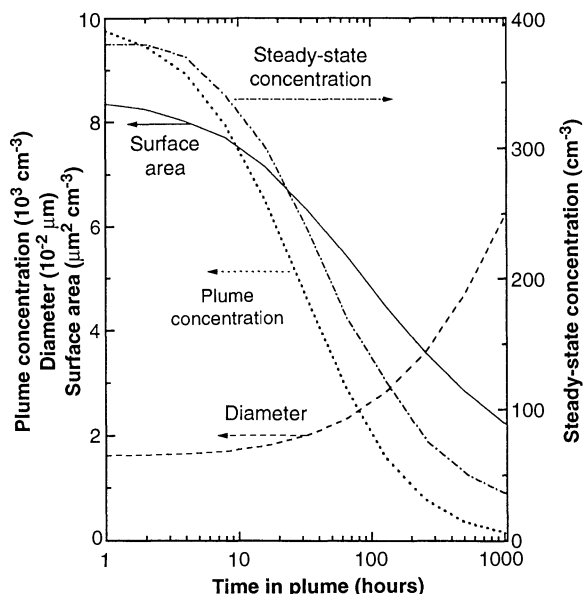
The observed OH peaks (Fig. 3) are largest for the early events (10 min), decreasing to negligible values for the oldest events (1 hour). In addition, the high reactivity of OH ensures that emitted OH was present for only a few seconds after emission from the engine (1, 21). Thus, an indirect source of OH that decreases with time is required to explain the observations. The most likely candidate is the photolysis of HONO, produced in the reaction of OH + NO within seconds of their emission from the engine (22, 23). The results of a photochemical model indicate that OH emission equal to 3 to 5% of the emitted NO is consistent with observed OH (23). The upper limit for emitted OH is likely to be within a factor of 2 of this value. Assuming

that the reaction of OH with  $\text{NO}_2$  controls  $\text{HNO}_3$  production in the plume, this OH estimate is consistent with the large  $\text{NO}_x/\text{NO}_y$  values cited above. Despite the additional source of OH in the plume, the decrease in  $\text{HO}_2$  concentrations is consistent with changes in the  $\text{HO}_x$  partitioning in the plume caused by increased NO (24).

Particles containing soot and  $\text{H}_2\text{SO}_4$  are expected in aircraft engine exhaust (25). Laboratory studies using the CN counter suggest that the volatile particles are composed of  $\text{H}_2\text{SO}_4$  and  $\text{H}_2\text{O}$ . Soot, which is not volatile at temperatures less than  $700^\circ\text{C}$ , may have been an important component of the nonvolatile fraction. The large measured EI for particles is surprising because fuel sulfur is thought to be emitted as  $\text{SO}_2$  rather than as  $\text{H}_2\text{SO}_4$  (25). The measured OH densities cannot explain oxidation of more than 1% of the  $\text{SO}_2$  in the plume (1, 23), whereas the minimum particle diameter detectable by the CN counter [ $0.009 \mu\text{m}$  (26)] and the observed concentrations require that at least 12 to 45% of the fuel sulfur (0.023 weight %) was oxidized to  $\text{H}_2\text{SO}_4$ . Thus, it is likely that  $\text{SO}_2$  was oxidized in the engine or through some other unexpected heterogeneous or gas-phase process after emission.

Heterogeneous chemistry occurring at a rate proportional to the surface area of sulfate aerosol is important in determining the atmospheric concentration of  $\text{NO}_x$  (9), which directly and indirectly controls the catalytic removal rate of  $\text{O}_3$  (27). With current fuels, a fleet of 500 HSCTs would increase the mass of sulfur in the lower stratosphere, but the change in aerosol surface area would depend on the fate of the sulfur emissions. If the emitted sulfur forms small particles soon after combustion, sur-

**Fig. 4.** Results from a coagulation model for the change in concentration, surface area, and mean particle diameter as a function of time. Initial conditions are chosen to match values observed for total aerosol particles observed near 1 hour. Subsequent values reflect the effects of coagulation when no mixing occurs. The remaining curve represents results of the box model for the steady-state particle concentration. At each point, the input to the box model is set by the corresponding results of the coagulation model scaled to a fleet of aircraft and mixed to a hemisphere-sized volume (29).



face area enhancements will be larger than if sulfur condenses on the existing background aerosol after dispersion and conversion to H<sub>2</sub>SO<sub>4</sub>. The differences depend largely on coagulation (collisions between liquid particles), which reduces both surface area and particle number over time. To estimate this difference, we included coagulation and condensation processes in a plume model (28) initialized with the CN observations at a plume age of 1 hour. All of the fuel sulfur was assumed to be oxidized to H<sub>2</sub>SO<sub>4</sub>, forming 70 weight % H<sub>2</sub>SO<sub>4</sub> and H<sub>2</sub>O particles with a mean diameter of ~0.016 μm. Over time, both surface area and number concentration decrease significantly in the undispersed plume (Fig. 4), whereas the mean particle diameter increases. The size and number distributions from the calculations were used as input to a box model to estimate the effects of a fleet of 500 HSCT aircraft with Concorde-like particle emissions (29). Dispersion of the plume to hemispheric scales slows coagulation, thereby extending particle lifetimes. In the absence of an accurate plume dispersion model (2), the full range of plume ages (1 to 1024 hours) was used to initialize the box-model calculations. The resulting particle concentrations at steady state vary from 380 to 35 cm<sup>-3</sup> for these respective ages. The corresponding range of steady-state aerosol surface is 2.0 to 1.8 μm<sup>2</sup> cm<sup>-3</sup>. The calculated steady-state values are large relative to background values of ~8 cm<sup>-3</sup> and ~0.8 μm<sup>2</sup> cm<sup>-3</sup>, respectively. If the same mass of sulfur is assumed to disperse before conversion to H<sub>2</sub>SO<sub>4</sub> and to condense on the existing background particles, total surface area increases to only 1.2 μm<sup>2</sup> cm<sup>-3</sup> (+50%) in the model.

In HSCT fleet scenario calculations, increasing particle surface area concentra-

tions from 125 to 150% as found above is likely to change the stratospheric O<sub>3</sub> perturbation. Local O<sub>3</sub> loss rates depend on NO<sub>x</sub>, and increasing surface area reduces the NO<sub>x</sub> fraction of the NO<sub>y</sub> reservoir (27). As a result, the concentration of NO<sub>x</sub> may actually decrease in the lower stratosphere if the scenario includes particle emissions with low NO<sub>x</sub> EI values. As an example, in a study of the coupling between HSCT NO<sub>x</sub> perturbations and volcanic aerosol loading (30), the combination of increased aerosol surface area (×4) and the emissions of a Mach 2.4 HSCT fleet changed O<sub>3</sub> column loss in broad mid-latitude regions from that obtained when aerosols are held at background values. Greater losses were found as the NO<sub>x</sub> emissions were lowered from 15 to 5 g NO<sub>x</sub> (kg fuel)<sup>-1</sup>. Thus, expected changes in stratospheric O<sub>3</sub> depend critically on the balance of the NO<sub>x</sub> EI and aerosol surface area perturbations. The change in aerosol surface area resulting from an HSCT fleet will be similar to enhancements observed following small volcanic eruptions. Enhancements in aerosol number concentrations decay rapidly following volcanic injections (31) but persist in steady state in the HSCT fleet calculations. The elevated number concentration of 3 to 10 times current background values will likely influence microphysical processes in polar stratospheric clouds, particularly those related to denitrification, a key parameter in the control of springtime polar O<sub>3</sub> loss (32).

Our measurements in the plume of the Concorde provide a comprehensive characterization of the emissions of a supersonic aircraft in flight. With a diverse set of instruments and only seconds of measurement time, we have addressed the EIs of gases and particles and the production of

nitric and sulfuric acids after the exhaust enters the atmosphere. If the EI of small particles is characteristic of the proposed HSCT fleet, significant increases in particle surface area and number are likely to occur, causing changes in O<sub>3</sub> loss processes at polar and mid-latitudes. Reducing this perturbation may require control of fuel sulfur, but at present we are uncertain about the processes controlling aerosol formation, so further study will be required before the efficacy of any control option can be determined reliably.

REFERENCES AND NOTES

1. R. C. Miake-Lye, W. J. Dodds, D. W. Fahey, C. E. Kolb, S. R. Langhoff, "Engine Trace Constituent Measurements Recommended for the Assessment of the Atmospheric Effects of Stratospheric Aircraft," ARI-RR-947 (Aerodyne Research, Inc., Billerica, MA, 1992).
2. *Global Ozone Research and Monitoring Project Rpt. No. 37* (World Meteorological Organization, Geneva, 1995); U. Schumann and D. Wurzel, in *Proceedings of an International Scientific Colloquium*, DLR-Mitteilung 94-06 (Deutsche Forschungsanstalt für Luft- und Raumfahrt, Köln, Germany, 1994).
3. R. S. Stolarski and H. L. Wesoky, Eds., *NASA Ref. Publ. 1313* (1993); D. L. Albritton et al., *NASA Ref. Publ. 1333* (1993).
4. R. Rosen and L. J. Williams, *Technol. Rev.* **96**, 22 (1993); P. S. Zurer, *Chem. Eng. News* **73**, 10 (24 April 1995).
5. H. S. Johnston, *Science* **173**, 517 (1971); P. J. Crutzen, *J. Geophys. Res.* **76**, 7311 (1971); H. S. Johnston, D. E. Kinnison, D. J. Wuebbles, *ibid.* **94**, 16351 (1989).
6. X. X. Tie et al., *J. Atmos. Chem.* **18**, 103 (1994); G. Pitari, V. Rizi, L. Ricciardulli, G. Visconti, *J. Geophys. Res.* **98**, 23141 (1993).
7. D. K. Weisenstein, M. K. W. Ko, J. M. Rodriguez, N.-D. Sze, *Geophys. Res. Lett.* **18**, 1991 (1991).
8. S. Bekki and J. A. Pyle, *ibid.* **20**, 723 (1993).
9. D. W. Fahey et al., *Nature* **363**, 509 (1993).
10. A. J. Broderick, A. K. Forney, D. W. Male, C. J. Scott, in "Propulsion Effluents in the Stratosphere: CIAP Monograph 2," DOT-TST-75-52 (National Technical Information Service, Springfield, VA, 1975), chap. 4.
11. D. W. Fahey et al., *J. Geophys. Res.* **100**, 3065 (1995).
12. S. C. Wofsy, R. C. Cohen, A. L. Schmeltekopf, *Geophys. Res. Lett.* **21**, 2535 (1994); J. M. Rodriguez, *Science* **261**, 1128 (1993).
13. P. Weisen, J. Kleffmann, R. Kurtenbach, K. H. Becker, *Geophys. Res. Lett.* **21**, 2027 (1994).
14. K. A. Boering et al., *ibid.*, p. 2567.
15. The calculation of an EI for a species from plume observations requires integrals (Δ) for CO<sub>2</sub> and the species and the carbon content of the fuel. An analysis of the Concorde fuel obtained after the flight showed the hydrogen and sulfur content of the Jet A-1 fuel to be 13.9 and 0.023 weight %, respectively (Aerospace Fuels Laboratory, Department of the Air Force, Kelly Air Force Base, Texas). The remaining 86.1 weight % is carbon, consistent with a C<sub>n</sub>H<sub>2n</sub> stoichiometry. The full oxidation of the carbon content of this fuel yields an EI for CO<sub>2</sub> of 3152 g CO<sub>2</sub> (kg fuel)<sup>-1</sup>. The EI for NO<sub>x</sub> is related to the EI for CO<sub>2</sub> as  

$$EI_{NO_x} = EI_{NO_y}$$

$$= \frac{46}{44} EI_{CO_2} \frac{\Delta NO_y \text{ (ppbv s)}}{\Delta CO_2 \text{ (ppmv s)}} 10^{-3} \text{ g NO}_x \text{ (kg fuel)}^{-1}$$
(2)
16. D. W. Fahey et al., *Nature* **345**, 698 (1990).

17. The concentration of  $\text{NO}_2$  is estimated from the photochemical steady-state relation involving the reaction with  $\text{O}_3$  and photolysis as

$$[\text{NO}_2] = [\text{NO}] \frac{k_{\text{NO-O}_3}[\text{O}_3]}{J_{\text{NO}_2}} \quad (3)$$

where brackets denote concentration,  $k_{\text{NO-O}_3}$  is the reaction rate coefficient of  $\text{O}_3$  with  $\text{NO}$ , and  $J_{\text{NO}_2}$  is the photolysis rate coefficient of  $\text{NO}_2$  to  $\text{NO}$  (17). This assumption can be made because the solar zenith angle is low ( $55^\circ$ ) and the plume age exceeds a few minutes. The reaction of  $\text{NO} + \text{ClO}$  does not contribute in Eq. 3 because  $\text{ClO}$  reacts with  $\text{NO}_2$  to form  $\text{ClONO}_2$  within a few minutes in the plume.

18. D. J. Hofmann and J. M. Rosen, *Geophys. Res. Lett.* **5**, 511 (1978).  
 19. M. R. Williams, in "Proceedings of the Second Conference on the Climatic Impact Assessment Program," DOT-TSC-OST-73-4, A. J. Broderick, Ed. (National Technical Information Service, Springfield, VA, 1973).  
 20. E. A. Brun, *Comité d'Études sur les Conséquences des Vols Stratosphériques (COVOS): Activités 1972-1976* (Société Météorologique de France, Boulogne, 1977).  
 21. R. C. Miake-Lye et al., *J. Aircr.* **30**, 467 (1991).  
 22. F. Arnold, J. Scheid, Th. Stimp, H. Schlager, M. E. Reinhardt, *Geophys. Res. Lett.* **19**, 2421 (1992).  
 23. T. Hanesco et al., in preparation.  
 24. In the lower stratosphere, the ratio of  $\text{HO}_2$  to  $\text{OH}$  is approximated by

$$\frac{[\text{HO}_2]}{[\text{OH}]} = \frac{k_{\text{OH-O}_3}[\text{O}_3]}{k_{\text{HO}_2+\text{NO}}[\text{NO}] + k_{\text{HO}_2+\text{O}_3}[\text{O}_3]} \quad (4)$$

where  $k_i$  are associated rate constants (27). By Eq. 4, the large decrease in  $\text{HO}_2$  in the plume is quantitatively consistent with the large  $\text{NO}$  values in the plume and  $\text{O}_3$  values that are unchanged from background values.

25. J. Zhao and R. P. Turco, *J. Aerosol Sci.*, in press; R. P. Turco et al., *J. Appl. Meteorol.* **19**, 78 (1980); R. C. Miake-Lye, R. C. Brown, M. R. Anderson, C. E. Kolb, paper presented at *Impact of Emissions from Aircraft and Spacecraft upon the Atmosphere*, Deutsche Forschungsanstalt für Luft- und Raumfahrt, Köln, Germany, 18 to 20 April 1994.  
 26. In addition to the CN counter, a particle spectrometer probe aboard the ER-2 measured the concentration of particles between 0.08 and 2  $\mu\text{m}$  in diameter. This instrument showed no response during the plume encounters, indicating that particles detected by the CN counter were smaller than 0.08  $\mu\text{m}$ .  
 27. P. O. Wennberg et al., *Science* **266**, 398 (1994).  
 28. F. Gelbard, and J. H. Seinfeld, *J. Colloid. Interface Sci.* **78**, 485 (1980).  
 29. The aerosol size distribution produced by the Concorde plume coagulation model for a given plume age (Fig. 4) is assumed to instantaneously mix into a volume representing the stratosphere poleward of  $20^\circ\text{N}$  and from 12 to 20 km in altitude. The particle number in the box volume is scaled to match particle emissions for the expected HSCT stratospheric fuel usage,  $70 \times 10^9 \text{ kg year}^{-1}$  (2, 8), and includes a steady-state background aerosol. The steady-state aerosol mass enhancement, from the input of aircraft-emitted sulfur and the 1-year removal time resulting from transport, is  $4.4 \times 10^{-11} \text{ kg m}^{-3}$ , approximately equal to the nonvolcanic background aerosol mass loading.  
 30. D. K. Weisenstein, M. K. W. Ko, J. M. Rodriguez, N.-D. Sze, *J. Geophys. Res.* **98**, 23133 (1993).  
 31. J. C. Wilson et al., *Science* **261**, 1140 (1993).  
 32. R. J. Salawitch et al., *ibid.*, p. 1146.  
 33. P. Newman, private communication.  
 34. K. R. Chan, S. G. Scott, T. P. Bui, S. W. Bowen, J. Day, *J. Geophys. Res.* **94**, 11573 (1989).  
 35. D. W. Fahey et al., *ibid.*, p. 11299.  
 36. R. S. Gao et al., *ibid.* **99**, 20673 (1994).  
 37. C. R. Webster et al., *Science* **261**, 1130 (1993).  
 38. K. K. Kelly et al., *J. Geophys. Res.* **94**, 11317 (1989).  
 39. J. C. Wilson, J. H. Hyun, E. D. Blackshear, *ibid.* **88**, 6781 (1983).  
 40. M. Loewenstein, J. R. Podolske, K. R. Chan, S. E. Strahan, *ibid.* **94**, 11589 (1989).  
 41. M. H. Proffitt et al., *ibid.*, p. 16547.  
 42. Experiments using the Concorde engine were per-

formed in a British high-altitude test cell at the National Gas Turbine Establishment in Pyestock, England, for the following conditions: Mach 1.95, 15.4 to 16.5 km, 227 K, stratospheric water vapor equivalent, and fuel flow of  $1.5 \text{ kg s}^{-1}$ . These results and theoretical calculations are part of the U.S. Climatic Impact Assessment Program (CIAP) (10).

43. Experiments were conducted on the Olympus 593 Mk 602 (production version) engine in a high-altitude test cell at the French Centre d'Essais des Propulseurs de Saclay of the Société Nationale d'Étude et de Construction de Moteurs d'Aviation for the following conditions: Mach 2.0, 16.2 km, 222 K, stratospheric water vapor equivalent, and fuel flow of  $1.6 \text{ kg s}^{-1}$ . These results are part of COVOS (20).

44. We appreciate the efforts of pilots J. Barrilleaux of NASA and F. Rude of Air France in acquiring this data set; Aerospace Fuels Laboratory of the U.S. Air Force in analyzing the fuel samples; J. A. Eilers, M. Craig, R. M. Stimpfle, and M. H. Proffitt for  $\text{ClO}$  and  $\text{O}_3$  data; D. K. Weisenstein and B. Massé for helpful discussions; and many others in France and New Zealand for ground support operations. K.A.B. acknowledges the support of a Global Change Distinguished Postdoctoral Fellowship from the U.S. Department of Energy. The High-Speed Research and Upper Atmosphere Research programs of NASA have supported this research.

28 April 1995; accepted 26 July 1995

## P'P' Precursors Under Africa: Evidence for Mid-Mantle Reflectors

Yves Le Stunff,\* Charles W. Wicks Jr.,† Barbara Romanowicz

Observations of precursors to P'P' from a recent exceptionally large deep earthquake in the Fiji Islands (moment magnitude = 7.6) at an array of broadband stations in California revealed mid-mantle reflectors near depths of 785 kilometers and 1200 kilometers under the southern African rift. Such observations, previously reported primarily in subduction zones, suggest that these reflectors may have a global character. Our analysis, which also indicated a sharp, uplifted 670-kilometer discontinuity, demonstrates the power of sparse regional broadband arrays for the study of weak, frequency-dependent features in deep-Earth structure.

Several studies around 1970 suggested the existence of steep velocity gradients or discontinuities at various depths in the Earth's mantle (830 km, 900 km, and 1200 km) and in various regions (1-3), but reference global Earth models developed since the 1970s have not found a compelling need for any of them. More recently, contrasts in seismic velocity or impedance have been identified near subduction zones at depths of 900 km (4-6) and 1200 km (6). The observation of precursors to PKPPK (P'P') has allowed investigation of mantle discontinuities of regions like Antarctica and the mid-Indian Ocean ridge with some success (2, 7, 8), but so far continents have been poorly sampled. The array-processing techniques appear to be the best for the detection of these phases (9-11); they enable us to suppress ambient noise and properly estimate the slowness of the seismic phases.

On 9 March 1994, a deep earthquake occurred in the Fiji islands [latitude,  $-18.039^\circ$ ; longitude,  $-178.413^\circ$ ; depth, 563 km; origin time, 23:28:06.7; moment magnitude ( $M_0$ ), 7.6], the largest in this region since the deployment of new generation broadband stations worldwide. This event was recorded on 22 broadband stations in

California (Fig. 1A). The location of the surface bounce points of P'P' follows a northeast-southwest trend south of Lake Tanganyika in a region where the African Rift is bending in a southeastern direction toward the Lake Malawi region (Fig. 1B). We now demonstrate the potential of the sparse broadband network to detect and characterize, in a wide frequency band, weak phases such as precursors to P'P' and identify discontinuities in the mantle. We use observations of the same event on the dense California short-period arrays (Fig. 1A) [Northern California Seismic Network (NCSN) and Southern California Seismic Network (SCSN)] to check the validity of the broadband observations in the common frequency band (0.2 to 5 Hz).

P'P' precursors have previously been observed at epicentral distances of  $\sim 70^\circ$  for which P'P' usually has high amplitude given the temporal proximity of arrivals of different core branches. Our stations lie in a range from  $76.4^\circ$  to about  $80.2^\circ$  where only the DF branch (which travels through the inner core) is expected to be seen. As our ray tracing experiments demonstrate (Fig. 2), this is an ideal distance range to look for mantle discontinuities at depths of 650 to 1100 km.

We stack the broadband (BB) and the short period (SP) arrays using three different bandpass filters: 3.5 to 12 s, 2.5 to 4 s, and 1.5 to 3 s (Fig. 3). In the bandpass 3.5 to 12 s for the BB stack (Fig. 3A), there are

Seismographic Station and Department of Geology and Geophysics, University of California at Berkeley, Berkeley, CA 94720, USA.

\*To whom correspondence should be addressed.

†Present address: Institut für Geophysik, D-37075 Göttingen, Germany.